Multi-faceted immunomodulatory and tissue-tropic clinical bacterial isolate potentiates prostate cancer immunotherapy

Anker et al.

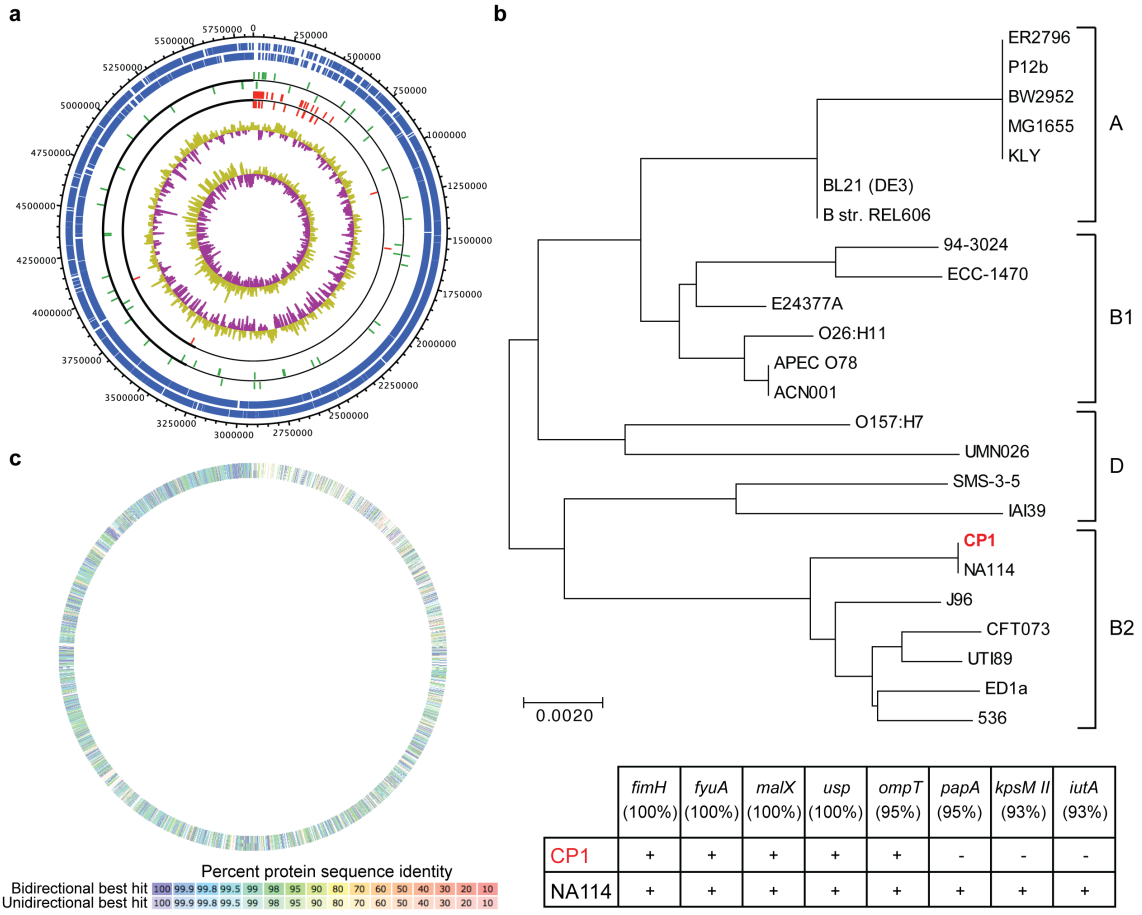

	fimH (100%)	*fyuA* (100%)	*malX* (100%)	*usp* (100%)	*ompT* (95%)	*papA* (95%)	*kpsM II* (93%)	*iutA* (93%)
CP1	+	+	+	+	+	-	-	-
NA114	+	+	+	+	+	+	+	+

Supplementary Figure 1. Whole genome sequencing of CP1. (**a**) The sequenced CP1 genome was visualized with Artemis DNAPlotter. Tracks from outermost to innermost: forward coding sequence (CDS), reverse CDS, forward tRNA, reverse tRNA, forward rRNA, reverse rRNA, GC plot, GC skew. (**b**) Phylogenetic tree of CP1 with reference *E. coli* strains using the Maximum Likelihood method with concatenated MLST sequences, constructed with MEGA7. Branch lengths were measured in the number of substitutions per site. Phylogenetic groups A, B1, D, or B2 are indicated. Table depicts the presence or absence of ST131 consensus virulence factor genes (with overall ST131 population prevalence indicated) in the CP1 or NA114 genomes. (**c**) Sequence comparison of the CP1 genome with the MG1655 genome, performed with RAST.

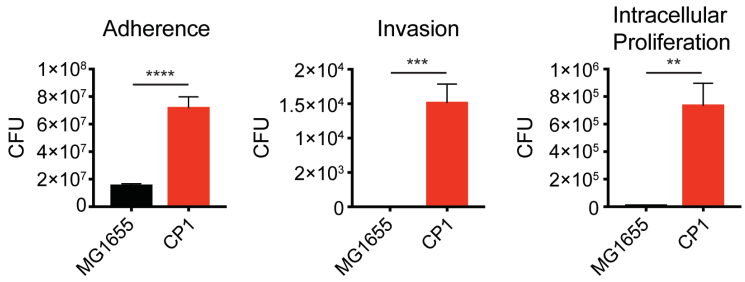

Supplementary Figure 2. CP1 adheres to, invades, and intracellularly proliferates within prostate cancer cells. (**a**) Gentamicin protection assay with CP1 and MG1655 with Myc-CaP cells *in vitro*, performed in sextuplicates, plated in serial dilutions. Data represented as mean ± S.E.M. Statistical significance was determined by Student's *t*-test. ** $P<0.01$, *** $P<0.001$, **** $P<0.0001$.

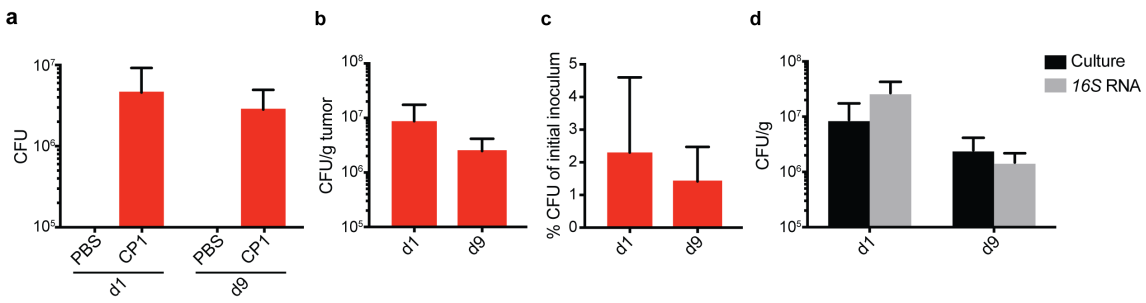

Supplementary Figure 3. Intra-tumoral CP1 is culturable and colonization levels remain constant over time. (**a**) Total bacterial colonization, (**b**) bacterial colonization normalized to tumor weight, and (**c**) bacterial colonization as a percentage of the original 2×10^8 CP1 inoculum, performed on day 1 (d1) and day 9 (d9) after intra-urethral PBS or CP1 administration to orthotopic Myc-CaP prostate tumor-bearing mice. (**d**) Bacterial colonization/g tumor as determined by both cultured tumor tissue and *16S* RT-PCR calibrated to CP1 counts on day 1 and day 9 after CP1 administration. Mice n = 4-5/group, tissue cultures plated in serial dilutions, technical duplicates, RT-PCR performed in technical duplicates. Data represented as mean ± S.E.M. Statistical significance was determined by (**a-c**) two-tailed Student's *t*-test, (**d**) two-way ANOVA.

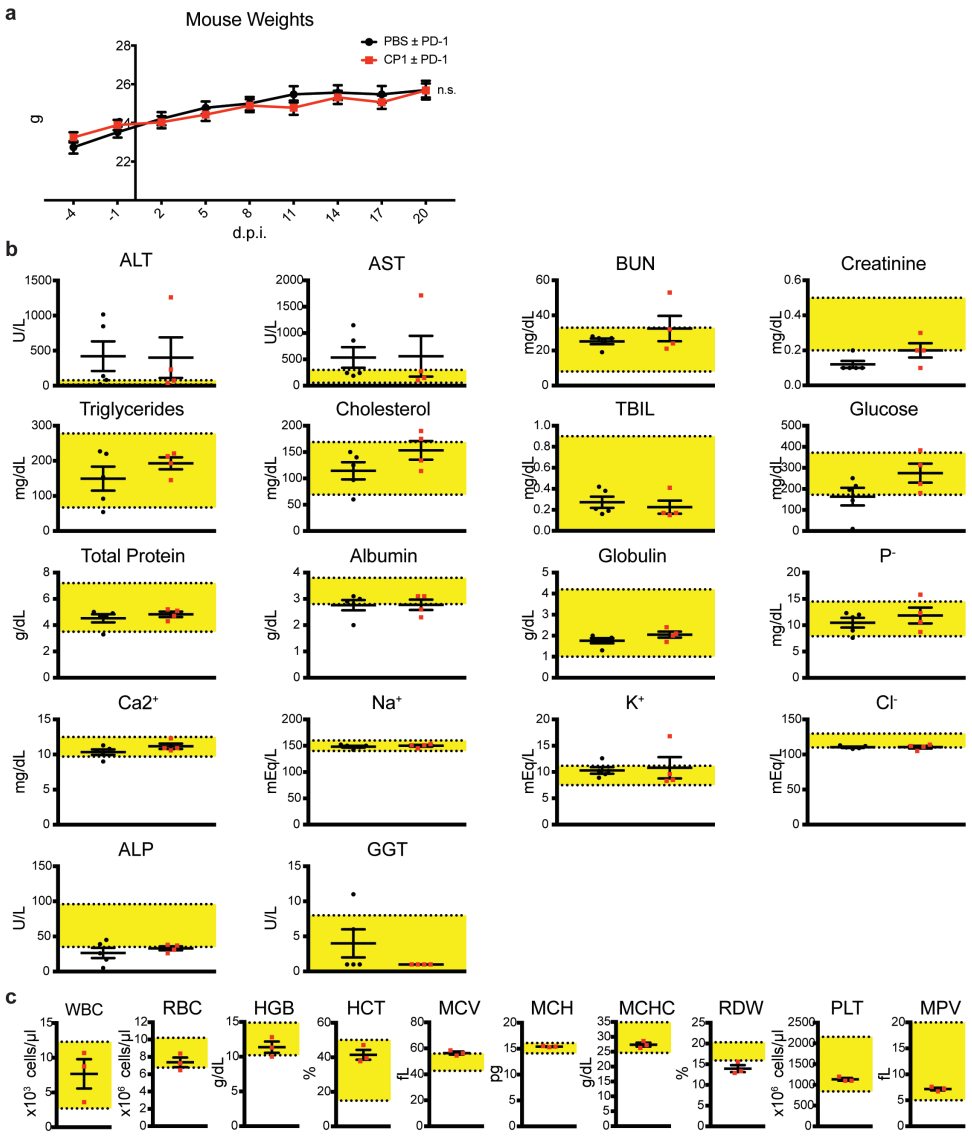

Supplementary Figure 4. CP1 does not cause any systemic toxicities. (**a**) Weights of PBS and CP1 administered mice (± anti-PD-1 antibody), plotted as days post-infection (d.p.i.), n.s. = not significant, *n* = 23-28 mice/experimental group. (**b**) Chemistry laboratory values of PBS and CP1 administered mice, yellow indicating the normal murine range (ALT = alanine aminotransferase, AST = aspartate aminotransferase, BUN = blood urea nitrogen, TBIL = total bilirubin, P^- = phosphorous, Ca^{2+} = calcium, Na^+ = sodium, K^+ = potassium, Cl^- = chloride, ALP = alkaline phosphatase, GGT = gamma glutamyl transferase), *n* = 4-5 mice/experimental group. (**c**) Complete blood count (CBC) values of CP1 administered mice, yellow indicating the normal murine range (WBC = white blood cell, RBC = red blood cell, HBG = hemoglobin, HCT = hematocrit, MCV = mean corpuscular volume, MCH = mean corpuscular hemoglobin, MCHC = mean corpuscular hemoglobin concentration, RDW = RBC distribution width, PLT = platelet count, MPV = mean platelet volume), *n* = 3 mice. Data represented as mean ± S.E.M. Statistical significance was determined by (**a**) two-way ANOVA, (**b**) two-tailed Student's *t*-test.

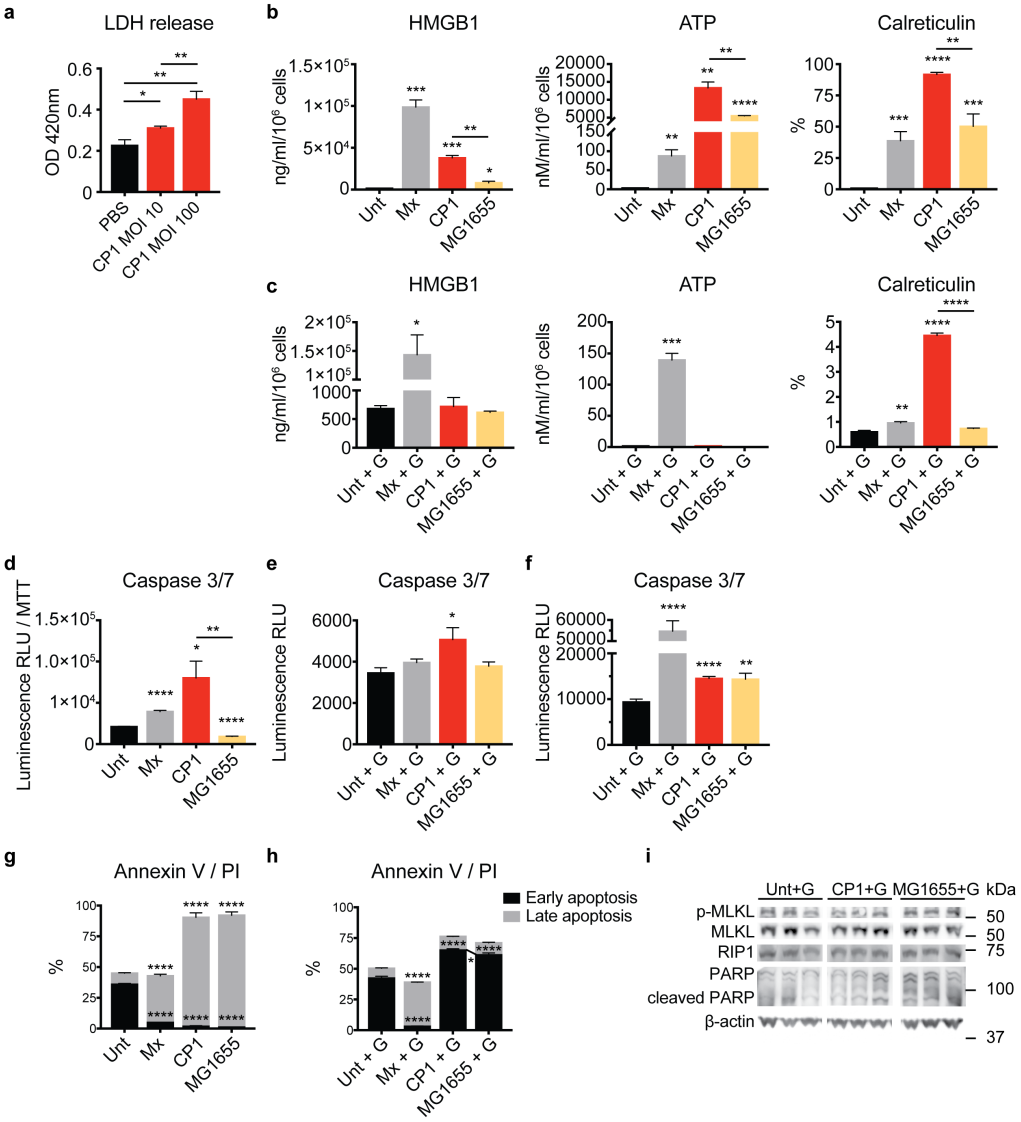

Supplementary Figure 5. CP1 induces ICD and select cell death markers, with and without gentamicin, and to a greater degree than MG1655. (**a**) LDH level, as a measure of cell death, from CP1 and Myc-CaP co-culture, performed in triplicates. (**b-i**) Myc-CaP cells were co-cultured with mitoxantrone (Mx), CP1 (MOI 1), or MG1655 (MOI 1) (**b, d, g**) in normal media or (**c, e, f, h, i**) with gentamicin (+ G) added after 2 hours. (**b, c**) ICD was measured via HMGB1 (ELISA, 72 hours), ATP (luminescence assay, 72 hours), and calreticulin (flow cytometry, 24 or 72 hours), performed in biological triplicates, technical duplicates. (**d-f**) Caspase 3/7 activity (luminescence assay, reported in relative light units [RLU]) was measured at (**d, e**) 6 hours or (**f**) 24 hours, (**d**) normalized to cell count (MTT assay), performed in sextuplicates. (**g, h**) Early stage apoptosis (Annexin V^+ PI^-) and late stage apoptosis (Annexin V^+ PI^+) were determined by flow cytometry after 24 hours, performed in triplicates. (**i**) Western blot analysis of phosphorylated and total MLKL, RIP1, full length and cleaved PARP, and β-actin after 24 hours, performed in triplicates. Data represented as mean ± S.E.M. Statistical significance was determined by two-tailed Student's *t*-test (each group compared to Unt, and CP1 compared to MG1655). * $P<0.05$, ** $P<0.01$, *** $P<0.001$, **** $P<0.0001$.

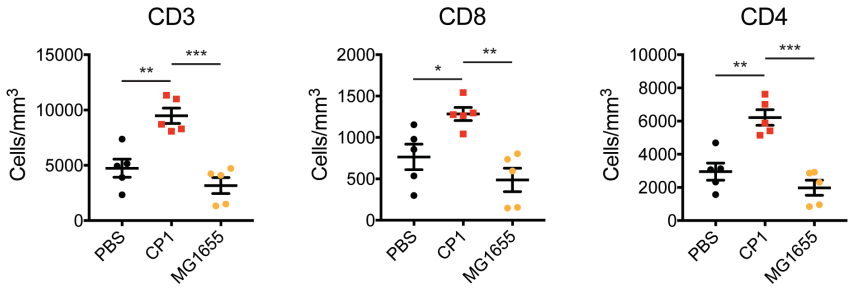

Supplementary Figure 6. Intra-urethrally administered MG1655 does not increase prostatic TILs. Flow cytometry analysis of orthotopic Myc-CaP tumors 9 days after intra-urethral administration of PBS, CP1, or MG1655, displayed as cell counts normalized to tumor volume. Mice n = 5/group. Data represented as mean ± S.E.M. Statistical significance was determined by two-tailed Student's t-test. * P<0.05, ** P<0.01, *** P<0.001.

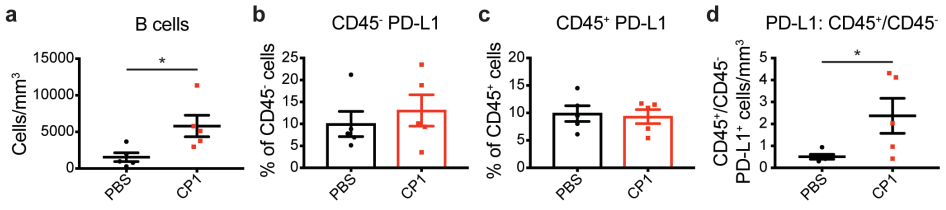

Supplementary Figure 7. CP1 increases B cells and does not increase PD-L1 expression. Flow cytometry analysis of (**a**) B cells, and PD-L1 on (**b**) $CD45^-$ and (**c**) $CD45^+$ intra-tumoral cells, and (**d**) the ratio of $CD45^+PD\text{-}L1^+/CD45^-PD\text{-}L1^+$ cell densities. n = 4-5 mice/experimental group, performed in 2 independent experiments. Data represented as mean ± S.E.M. as cell counts normalized to tumor volume (scatter plots) or percentages of parent gate (scatter boxed plots). Statistical significance was determined by two-tailed Student's t-test. * P<0.05.

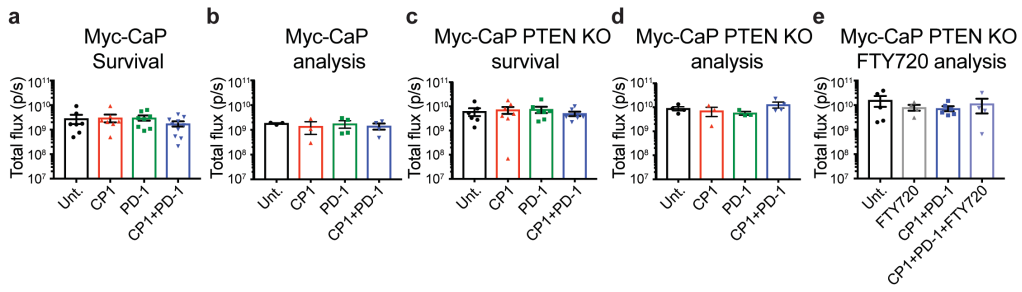

Supplementary Figure 8. Normalization of orthotopic pre-treatment tumor burden in all *in vivo* experiments. Pre-treatment tumor IVIS quantification of Unt., CP1, anti-PD-1 antibody, and combination CP1 and anti-PD-1 antibody treated mice in (**a**) Myc-CaP survival (Figure 4a,b, Supplementary Figure 9, Supplementary Figure 10a), (**b**) Myc-CaP analysis (Figure 4b-e), (**c**) Myc-CaP PTEN KO survival (Figure 5e), (**d**) Myc-CaP PTEN KO analysis (Figure 5f, Figure 6, Supplementary Figure 10b, Supplementary Figure 12), and (**e**) of Unt., FTY720, combination CP1 and anti-PD-1 antibody, and combination CP1 and anti-PD-1 antibody and FTY720 treated mice (Figure 7). Data represented as mean ± S.E.M. Statistical significance was determined by one-way ANOVA.

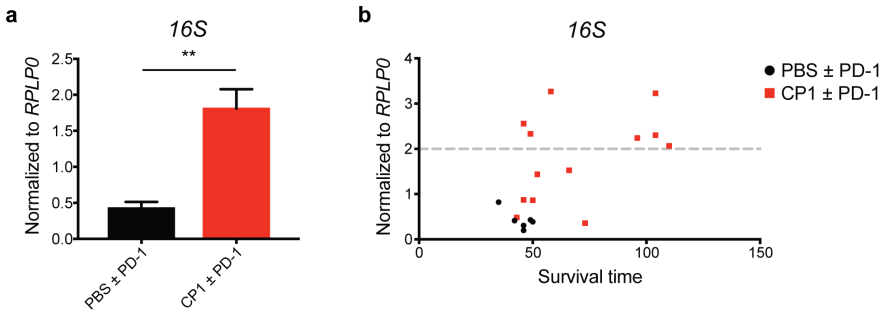

Supplementary Figure 9. CP1 load is linked to treatment efficacy. *16S* qRT-PCR of Myc-CaP survival mice tumors (**a**) at their endpoints and (**b**) plotted over time after tumor injection, dotted line indicates cutoff for high CP1. Data represented as mean ± S.E.M. Statistical significance was determined by two-tailed Student's *t*-test. ** $P<0.01$.

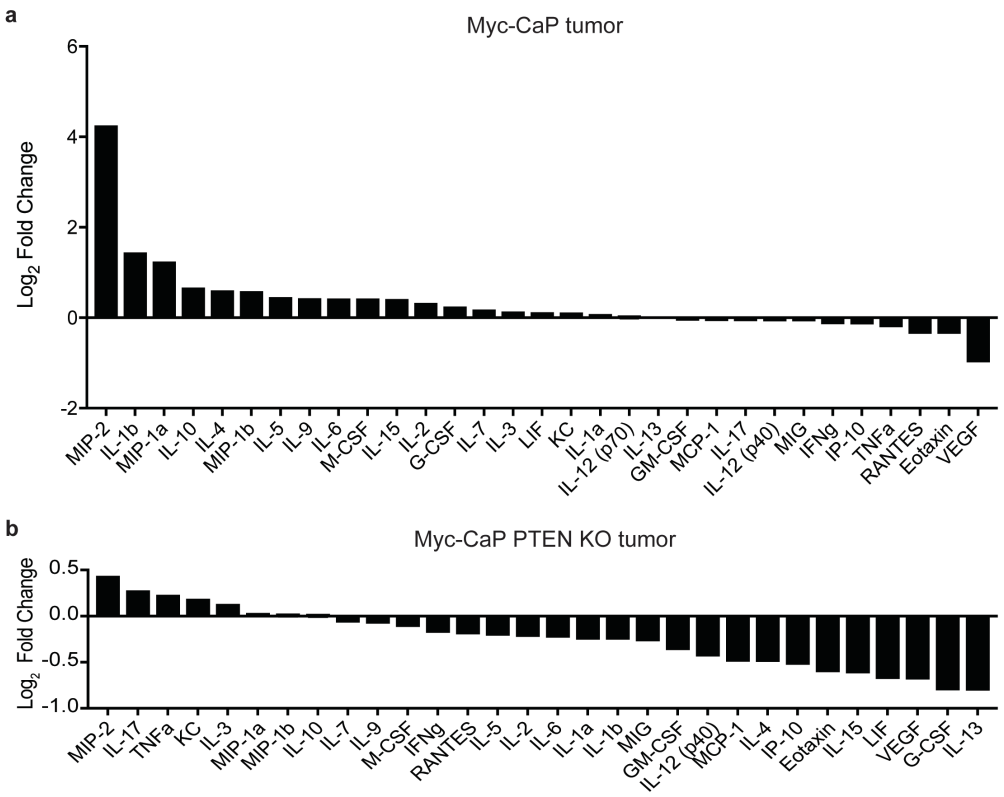

Supplementary Figure 10. CP1 decreases intra-tumoral VEGF, increases pro-inflammatory cytokines and chemokines. Multiplex cytokine and chemokine array from (**a**) Myc-CaP survival tumors, performed with n = 11-12 mice/experimental group, and from (**b**) Myc-CaP PTEN KO tumors, performed with n = 5-6 mice/experimental group and technical duplicates. Data represented as $\log_2$ fold change with and without CP1 administration.

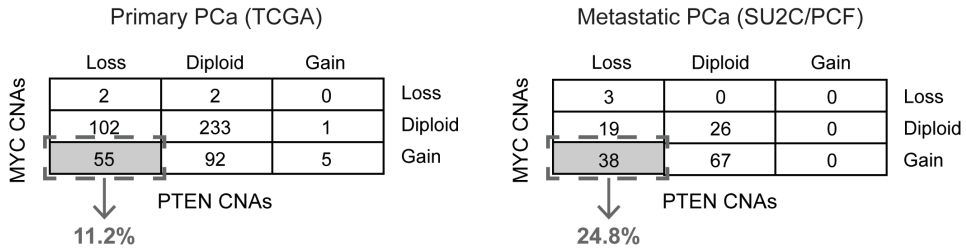

Supplementary Figure 11. Concurrent *MYC* copy number gain and *PTEN* copy number loss represents advanced human prostate cancer. Tables of the number of samples with *MYC* and *PTEN* copy number diploid, loss, or gain in the TCGA and SU2C/PCF databases, with gray numbers indicating the percent of samples with concurrent *MYC* gain and *PTEN* loss.

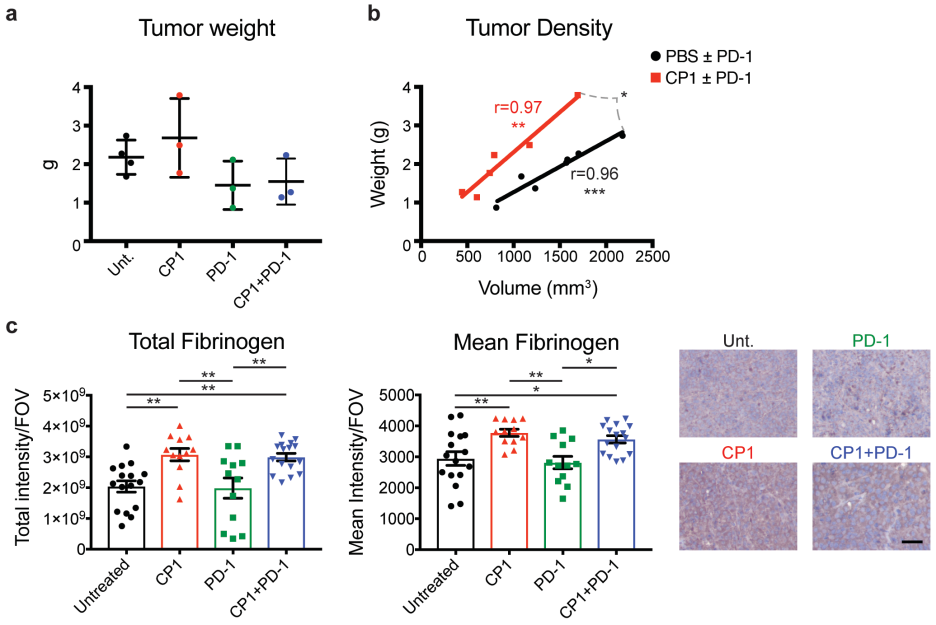

Supplementary Figure 12. CP1 increases tumor density via fibrinous exudate. Myc-CaP PTEN KO tumor (**a**) weights, *n* = 3-4 mice/experimental group and (**b**) densities, *n* = 6-7 mice/experimental group. (**c**) Fibrinogen IHC quantified by total and mean positivity/FOV and representative images, quadruplicate FOVs scored per sample, scale bar: 50µm, *n* = 4-6 mice/experimental group. Data represented as mean ± S.E.M. or linear regression trend lines**.** Statistical significance was determined by (**a**) two-tailed Student's *t*-test, (**b**) Pearson's correlation coefficient (r) an ANCOVA comparing slopes of trend lines, (**c**) one-way ANOVA. * $P<0.05$, ** $P<0.01$, *** $P<0.001$.

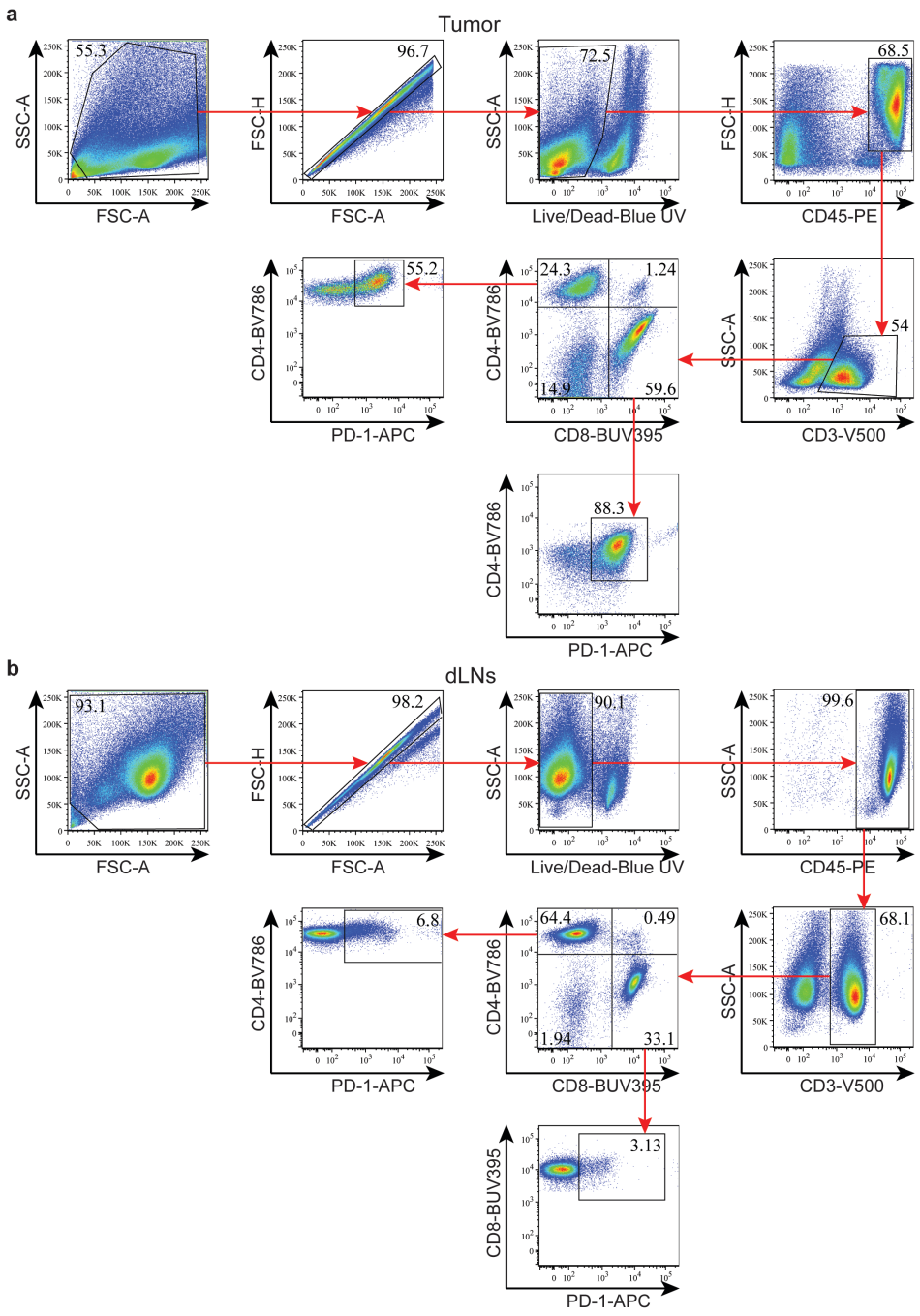

Supplementary Figure 13. Representative flow cytometry gating strategy. For all flow cytometry analyses, initial gating was performed on overall morphology, singlets, live cells, and CD45^{+} cells, followed by antigens of interest, from (**a**) tumors or (**b**) dLNs. SSC-A = Side Scatter-Area, FSC-A = Forward Scatter-Area, FSC-H = Forward Scatter-Height.

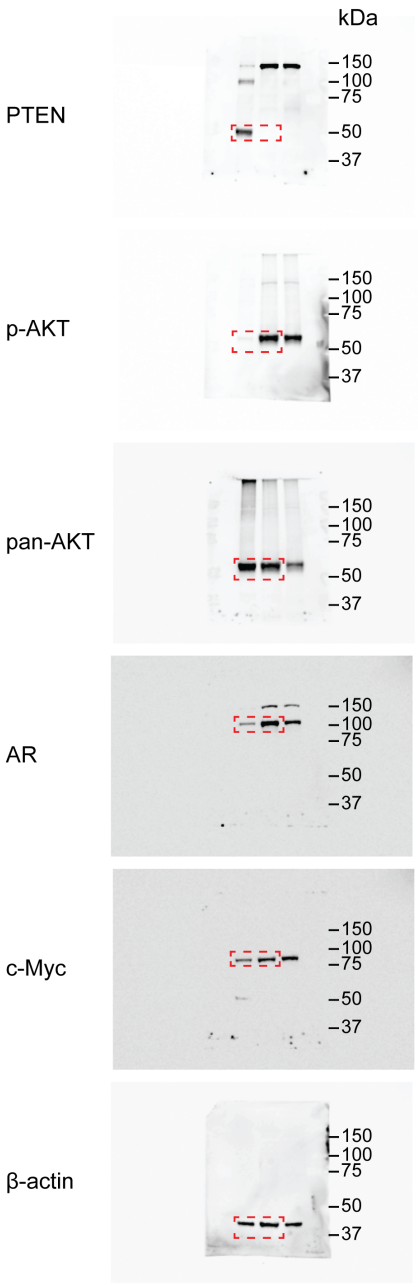

Supplementary Figure 14. Uncropped images of western blots from Figure 5a. Lane 1 is Myc-CaP, lane 2 is Myc-CaP PTEN KO, lane 3 is a second Myc-CaP PTEN KO clone (not included in Fig. 5a or in subsequent experiments). Red boxes represent the cropped images displayed in Fig. 5a.

Supplementary Table 1. Primary antibodies used in this study for flow cytometry.

Antigen (mouse)	Label	Clone	Vendor	Catalog #
Calreticulin	Unconjugated		Abcam	ab2907
Annexin V	FITC		eBioscience	11-8005
PI	-		eBioscience	00-6690
CD45	PE	30-F11	BD	553081
CD3ε	V500	500A2	BD	560771
CD4	BV786	RM4-5	BD	563727
CD8α	BUV395	53-6.7	BD	563786
CD25	BV421	PC61	BD	562606
FoxP3	eFluor 660	FJK-16s	eBioscience	50-5773-80
CD11b	Alexa Fluor 700	M1/70	BD	557960
Gr-1	BUV395	RB6-8C5	BD	563849
γδ TCR	BV421	GL3	BD	562892
NKp46	Alexa Fluor 700	29A1.4	BD	561169
B220	BV786	RA3-6B2	BD	563894
F4/80	BV421	T45-2342	BD	565411
CD11c	BV786	HL3	BD	563735
CD80	FITC	16-10A1	BD	563727
CD107a	BV786	1D4B	BD	564349
IFNγ	Alexa Fluor 488	XMG1.2	BioLegend	505813
TNFα	Alexa Fluor 700	MP6-XT22	BD	558000
IL-17A	BUV395	TC11-18H10	BD	565246
Granzyme B	eFluor 450	NGZB	eBioscience	48-8898-80
Perforin	APC	eBioOMAK-D	eBioscience	17-9392-80
PD-1	APC	J43	BD	562671
PD-L1	APC	10F.9G2	BioLegend	124312
PD-L2	BV421	TY25	BD	1564245
CD95	BV421	Jo2	BD	562633
CD95L	APC	MFL3	eBioscience	17-5911-80

Supplementary Table 2. Primary antibodies used in this study for histology.

Antigen (mouse)	Dilution	Protocol	Clone	Vendor	Catalog #
E. coli	1:500	IF		Abcam	ab20640
HMGB1	1:1000	IF		Abcam	ab18256
Calreticulin	1:500	IF		Abcam	ab2907
CD3ε	1:100	IHC	CD3-12	Bio-Rad	MCA1477T
CD3ε	Pre-diluted	IHC	2GV6	Ventana	790-4341
Fibrinogen	1:200	IHC	ab34269	Abcam	ab34269

Supplementary Table 3. Primary antibodies used in this study for western blot.

Antigen (mouse)	Dilution	Clone	Vendor	Catalog #
p-MLKL	1:1000	EPR9515(2)	Abcam	ab196436
MLKL	1:1000		Abcam	ab172868
RIP1	1:1000	38/RIP	BD Biosciences	610458
PARP	1:1000	H-250	Santa Cruz Biotechnology	sc-7150
PTEN	1:1000	138G6	Cell Signaling	9559
p-AKT	1:1000	S473	Cell Signaling	4060
pan-AKT	1:1000	C67E7	Cell Signaling	4691
AR	1:2000	N-20	Santa Cruz Biotechnology	sc-816
c-Myc	1:1000	Y69	Abcam	ab32072
β-actin	1:3000	AC-74	Sigma	A5316